JAMES D. KINNISON, RICHARD H. MAURER, and THOMAS M. JORDAN

ESTIMATION OF THE CHARGED PARTICLE ENVIRONMENT FOR EARTH ORBITS

A description of the charged particle environment seen in Earth orbit by spacecraft is presented. This includes the effects of trapped protons and electrons, solar protons, and galactic cosmic rays. A methodology for ensuring that satellite systems can withstand the effects of these particles is proposed, and the methods and the computer tools developed to predict the effects of charged particles on spacecraft systems are given.

INTRODUCTION

Spacecraft in Earth orbit are subject to many environmental stresses. Compromise in system design needed to ensure the survivability of a satellite is often the most important constraint on the performance of a satellite system. Many design trade-offs stem from the conflict between a desired system capability and a known problem withstanding environmental conditions. The resolution of this conflict usually costs weight and power or limits the performance of a satellite system. Accurate prediction of these constraints is important to avoid needless limitations on spacecraft systems.

One difficult task facing a satellite system designer is radiation hardness assurance. Charged particles found in space cause many problems that must be overcome. For electronic systems, these problems are total dose degradation owing to protons and electrons found in the Van Allen belts or solar flares; single-event phenomena caused by heavy ions found in galactic cosmic rays, solar protons, and trapped protons; and displacement damage effects on solar cells and sensors. Total dose degradation is an aging process that limits the lifetime of an electronic device. Single-event problems include latchups, which are destructive, and soft errors (bit flips). These latter effects are normally seen as an increase in system noise or as a temporary loss of data. Displacement damage causes loss of efficiency and power in solar cells. It also causes increases in dark current and decreases in charge transfer efficiency in star cameras and charge-coupled devices.

The problem of hardness assurance can be separated into two different tasks. First, we need to understand the changes in electrical devices caused by charged particles. These effects have been well studied and are not discussed here. Second, we must generate an accurate estimate of the space radiation environment. Models that adequately predict the environment impinging on the surface of a satellite are available. These models, however, do not include the attenuation of incident particles due to spacecraft structure, nor do they include an estimate of the single-event upset rate for a device in a given orbit. Two tools have been created to provide the information needed to adequately protect spacecraft systems without undue constraint: NOVICE, a computer program written by Thomas M. Jordan, which uses a three-dimensional geometrical model of a spacecraft to predict the dose at any point within the spacecraft; and MERGE, a Monte Carlo computer simulation written by James D. Kinnison, which predicts the single-event upset and latchup rate of devices caused by galactic cosmic rays. The following discussion examines the orbital charged particle environment and describes the models typically used to estimate the flux external to a satellite. A treatment of the tools devised by the authors that provides additional information not included in earlier models follows. We also offer several examples of satellite systems that have benefited from these new models.

TRAPPED PARTICLES

Most charged particles that affect satellite systems are found in the Van Allen radiation belts, which were discovered in 1958 by Van Allen et al.[1] when Geiger counters aboard Explorer I and Explorer III saturated because of high radiation flux. These belts consist of electrons and protons trapped by the Earth's magnetic field in a distorted toroid having longitudinal symmetry around the geomagnetic pole. The energy and spatial distributions of particles undergo both regular and irregular variations with time, and although theoretical studies have described the particle trapping mechanisms, a complete theoretical description of the belt dynamics is not feasible.

The Earth's magnetic field in the radiation belt region can generally be described by a dipole located near the center of the Earth and directed so that the Earth's magnetic north pole is located on the surface in northern Greenland. The geomagnetic field is often described by two coordinate systems: the R–λ system, where R is the distance from the Earth's center and λ is the geomagnetic latitude; and the B–L coordinate system, which describes the field in terms of the field strength B and McIlwain's parameter L. These systems avoid the inaccuracies brought on by the dipole model of the Earth's field and allow the use of spherical harmonic expansions of the field. They are related to first order through the following set of equations:

$$R = L \cos^2\lambda \qquad (1)$$

and

$$B = \frac{B_0}{R}\left(4 - \frac{3R}{L}\right)^{1/2}, \qquad (2)$$

where B_0 is the field strength at the Earth's surface on the equator, 3.12×10^{-5} T. Figure 1 shows the magnetic field in both the B–L and R–λ systems.[2]

As described by Alfvén and Falthammar,[3] a charged particle in a dipole field experiences three distinct quasi-periodic motions: gyration around the field lines, bounce between conjugate mirror points, and azimuthal drift around the Earth. For a proton of given energy on an arbitrary L shell, the gyration frequency is greater than the bounce frequency by about 2 orders of magnitude, and the bounce frequency exceeds the drift frequency by about 4 orders of magnitude; the differences are greater for electrons.[4] Since the frequencies of motion are so different, the motions are largely uncoupled. The combined effect of these three types of motions is to confine particles to shells within the Earth's magnetic field. In the B–L coordinate system, these shells are surfaces of constant L. A qualitative picture of the three motions is given in Figure 2 (Ref. 5).

Theoretical models that give the energy and spatial distribution of trapped particles are based on the solution of transport equations for the belts with suitable boundary conditions. A time-dependent model would require a set of time-dependent boundary conditions, however. Since these are not currently available, most theoretical models are solved for steady-state conditions. But these models are rarely used for total dose estimates because the calculations involved are difficult and time-consuming.

Empirical models of the Van Allen radiation belts are based on satellite measurements compiled over the last three decades. The most recent of these, AP-8 (Ref. 6) and AE-8 (J. I. Vette, private communication), provide time-averaged omnidirectional electron and proton fluxes as a function of energy and spacecraft position. The data can then be used to calculate orbit-averaged

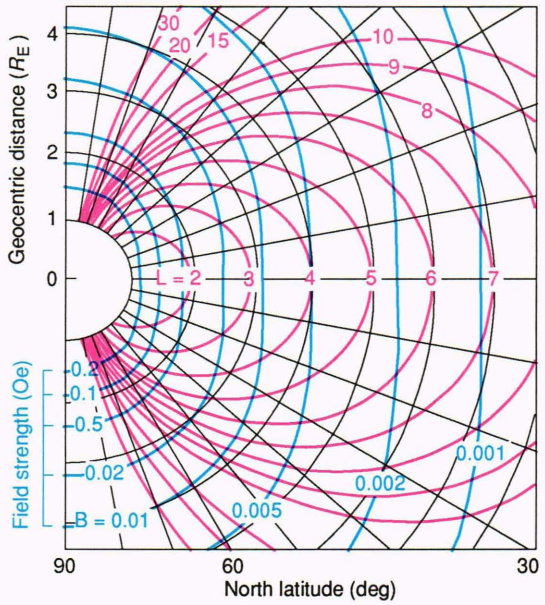

Figure 1. Geomagnetic field coordinates, B and L, as functions of latitude and distance from the Earth's center.

spectra. Neither AP-8 nor AE-8 includes short-term variations, diurnal variations, or other effects, however; each is a simplification of the actual radiation belt behavior.

AP-8 provides a model of the trapped proton flux with energies between 0.1 and 400 MeV. Since the spatial and energy distributions of the belts are changed by solar activity, two versions of the model are given, one for solar maximum conditions and one for solar minimum conditions. From these data, a picture of the gross characteristics of the trapped proton belt can be found. Figure 3 is a plot of the omnidirectional proton flux (energy > 10 MeV) averaged over four circular orbits as a function of orbital altitude and inclination during solar maximum conditions. Figure 4 shows a typical flux spectrum near the region of highest proton concentration.

Electron models for solar minimum and maximum conditions are given in AE-8. The features of this model are shown in Figure 5. Again, this figure is a plot of the omnidirectional electron flux (energy > 0.25 MeV)

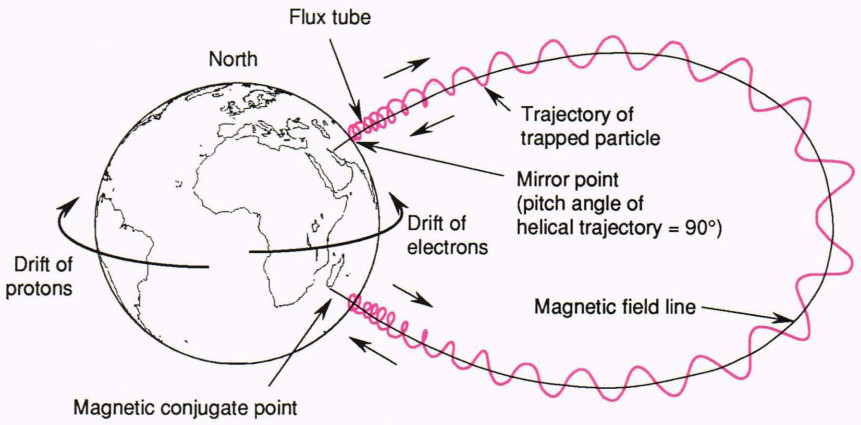

Figure 2. Depiction of the three motions exhibited by trapped particles.

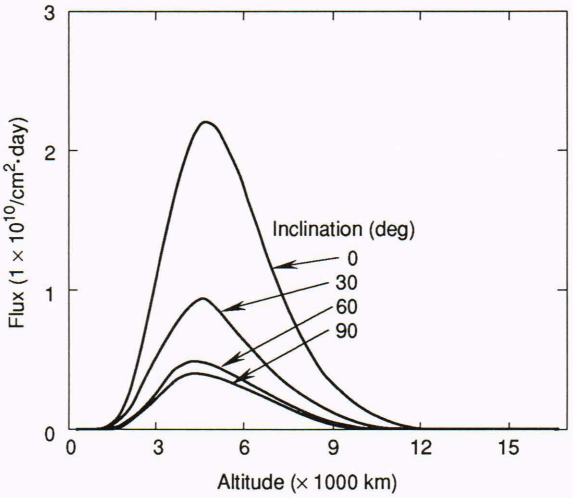

Figure 3. Proton flux greater than 10 MeV integrated over circular orbits as a function of alititude and inclination.

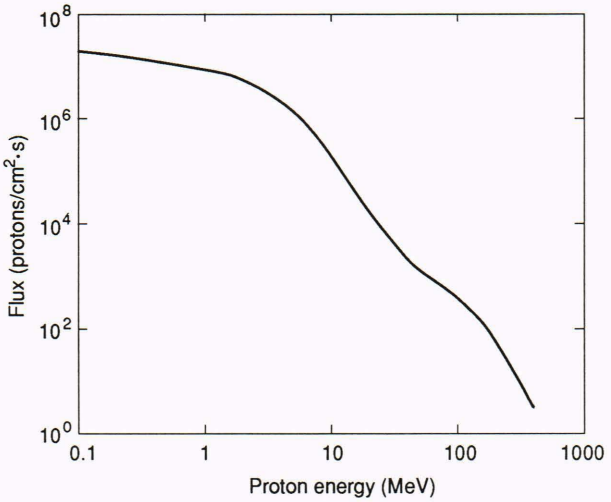

Figure 4. Proton flux as a function of energy for $L = 2$ in the equatorial plane.

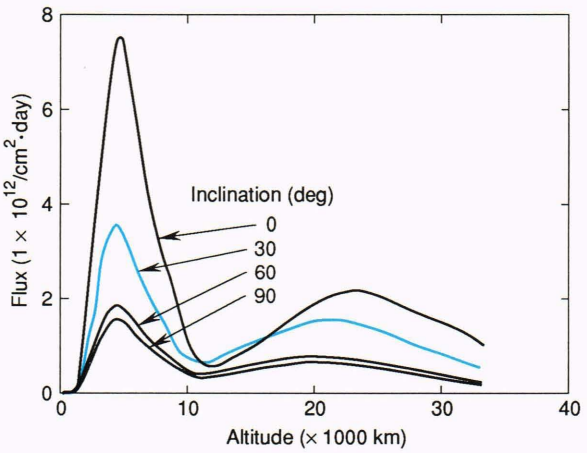

Figure 5. Electron flux greater than 0.25 MeV integrated over circular orbits as a function of altitude and inclination.

averaged over four circular orbits as a function of altitude and inclination. Unlike the proton belt, electrons are mostly found in two regions, called the inner and outer belts. Figure 6 is a typical electron flux spectrum near the peak of the inner belt in the equatorial plane.

Anomalies exist in the spatial distribution of the trapped particles around the Earth. The most important of these for spacecraft operations is the South Atlantic Anomaly (SAA). Because the center of the Earth's magnetic field is displaced from the geographic center, the fluxes of trapped particles at low altitudes are larger over the southern Atlantic Ocean than anywhere else at the same altitude. In effect, the magnetic field is weakest in this geographic region, and so the trapped particles encounter their lowest mirror point there. Particles constantly move across this region and are swept out of the Van Allen belts by interactions with the atmosphere. For satellites in Earth orbit below 1000 km, the total dose environment is dominated by the particles in the SAA. Figure 7 is a contour plot of the anomaly[5] at an altitude of 750 km for protons with energies between 5 and 7 MeV.

SOLAR FLARE PARTICLES

Until quite recently, the high-energy solar proton fluence model used most often in total dose calculations was that developed by King.[7] But this model was designed specifically to make predictions about the twenty-first solar cycle during the period 1977–83 on the basis of data from the twentieth solar cycle. Feynman et al.[8] have now shown that the assumptions made by King for the twenty-first cycle invalidate the use of his model for any other solar cycle, particularly since the twentieth cycle contained only one large event (the famous August 1972 event). The distribution of proton fluences greater than 10 MeV was such that a single mathematical distribution could not be used to characterize both the twenty-four "ordinary" events and the one "anomalously large" event of the twentieth cycle.

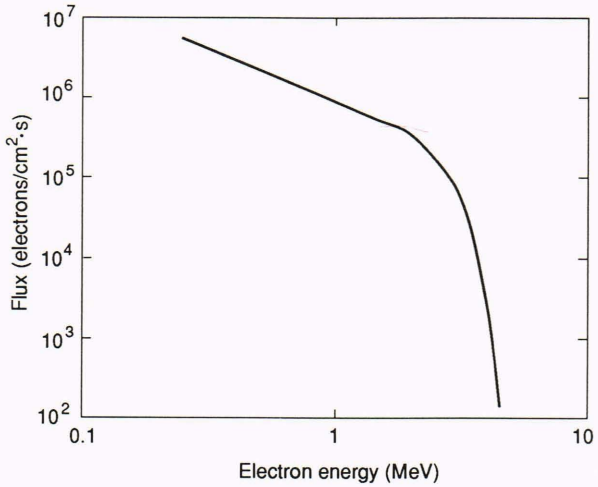

Figure 6. Electron flux as a function of energy for $L = 4$ in the equatorial plane.

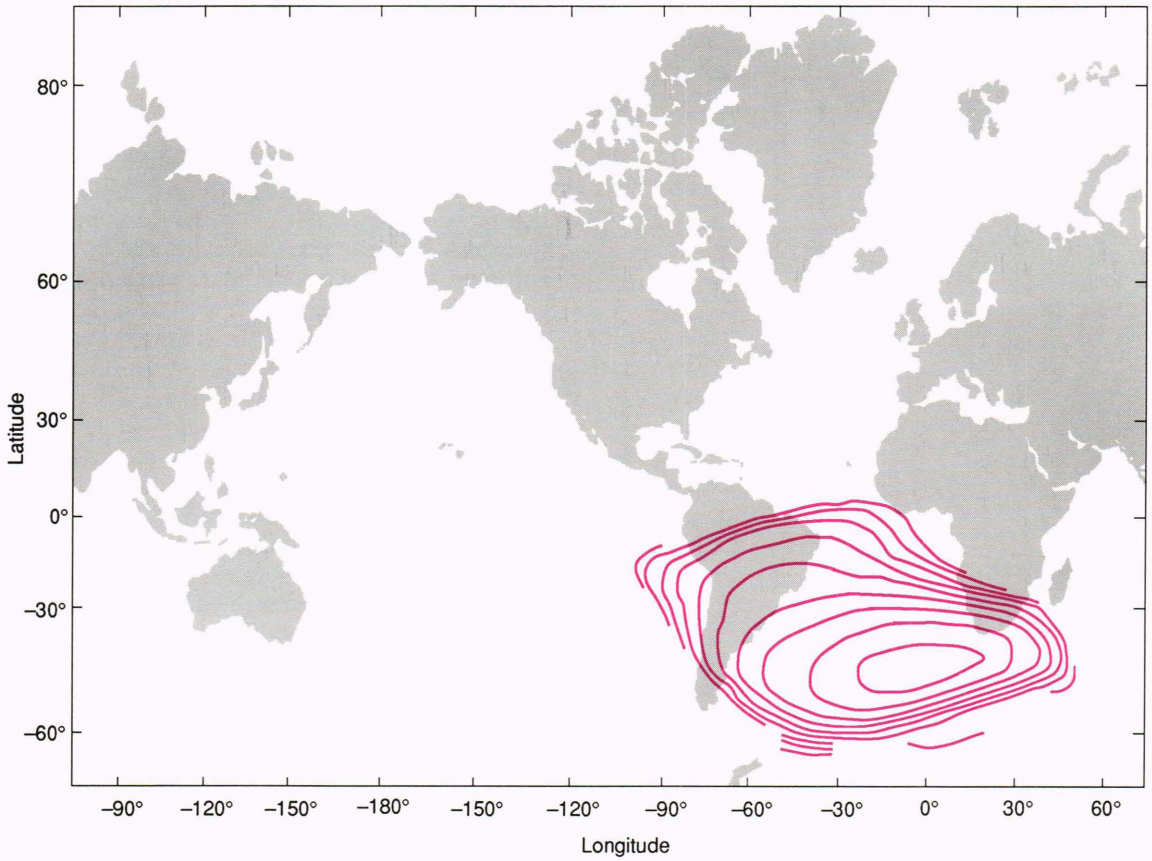

Figure 7. Proton flux contours in the South Atlantic Anomaly at an altitude of 750 km. The contours depict a proton flux of 28 to 45 MeV in particles/cm^2·s·MeV.

Feynman and colleagues[8,9] have reviewed all the energetic solar proton data from 1956 to 1985, three complete solar cycles. They used observations from riometers, rockets, and balloons for 1956 through 1962, and interplanetary spacecraft data from the Interplanetary Monitoring Platform (IMP 1 through 3 and 5 through 8), in addition to data from the Orbiting Geophysical Observatory (OGO 1) for 1963 through 1985. Events in the second time period were defined as having proton fluence (>10 MeV) larger than 10^7 particles/cm^2 or proton fluence (>30 MeV) larger than 10^5 particles/cm^2. Events totaled 120 above the first energy and 140 above the second.[9]

Significantly, the distinction between ordinary and anomalously large events disappears when all three solar cycles are combined; that is, the August 1972 event is no longer an outlier with respect to proton fluence distributions. The 1960 event actually has the highest proton fluence, and two 1989 events in cycle twenty-two, those of August and September, have >10 MeV proton fluences within factors of 4 and 2, respectively, of the 1972 event. The 1989 events were not included in the original modeling by Feynman et al. but helped validate their conclusions.

An epochal analysis of the solar cycle variation of the annual flux was also carried out. The results show that the solar cycle can be divided into four inactive years of low annual fluence and seven active years with annual fluences greater than 5×10^7 particles/cm^2 (>10 MeV). The active period extends from two years before sunspot maximum to four years after maximum. The times of sunspot maximum determined by Feynman et al. are 1957.9, 1968.9, 1979.9, and 1990.9 for the nineteenth, twentieth, twenty-first, and twenty-second cycles, respectively. Active years proved to have fluences greater than 5×10^7 particles/cm^2 (>10 MeV), even if no major proton event occurred during that particular year.

When we evaluate the distribution of proton event fluences, we find that minimum or inactive years have such low fluence that only the seven active years need to be modeled. This result enables Feynman et al. to achieve a better statistical fit with a log normal distribution to events, with proton fluences larger than the modal fluence. No division between ordinary and anomalous events exists, and events from several solar cycles can be used to obtain an adequate sample of event fluences. Figure 8 shows the solar cycle dependence of annual fluence for the years 1956 through 1986.

Using the log normal distribution for large events, Feynman et al. performed a Monte Carlo calculation to determine the probability that a given spacecraft mission will experience a solar proton fluence above a given level. These probabilities were calculated for mission lengths of one to seven active years. Results are shown in Figures

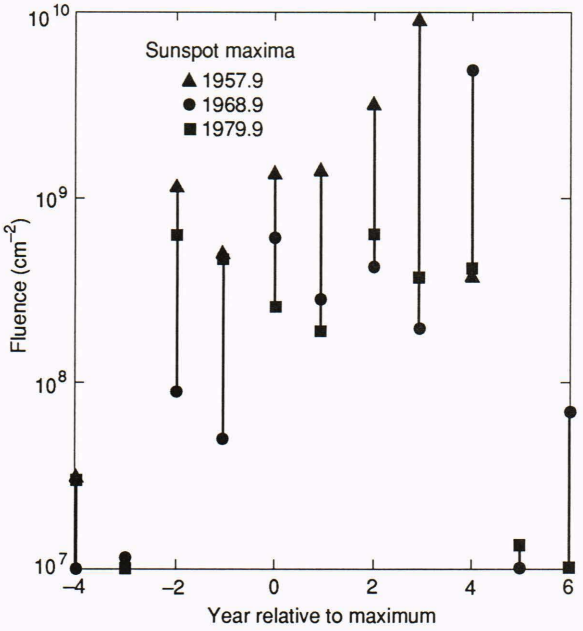

Figure 8. Solar cycle variation of the annual integrated fluence of solar proton events at the Earth. (Reprinted, with permission, from Ref. 9: © 1990 by American Institute of Aeronautics and Astronautics.)

9A and 9B for >10 MeV and >30 MeV fluence, respectively. The >10 MeV fluence expected with the new model is about twice that expected by the earlier models; the >30 MeV fluence is about the same. For example, for a mission lasting one solar active year, the chance of seeing >10 MeV fluence exceeding 7.7×10^{10} particles/cm^2 is 2%, while for seven active years, the probability increases to 40%.

The effect of these new results on spacecraft hardware is seen primarily on the least shielded subsystems. Primarily, the increased >10 MeV proton fluence will cause greater proton-displacement-damage degradation of solar cells. Since the >30 MeV fluence is about the same as that of the older models, the total dose and single-event effects predicted owing to this more penetrating component of the solar proton spectrum will be quite similar to predictions of the older models.

TOTAL DOSE ESTIMATION

The process by which a total dose estimate is obtained can be broken down into two distinct steps. The first is to calculate an integrated flux spectrum for each particle type of interest. This information depends on such factors as the spacecraft orbit and the mission epoch, and represents the environment external to the spacecraft. Radiation effects in microelectronics are rarely studied in terms of particle flux, however. A more convenient unit is the rad, a measure of the energy deposited in a material, defined as 10^{-8} J/kg. The second step, then, is to convert the flux spectrum into dose at interesting points within the spacecraft. Accounting for particle attenuation caused by factors such as spacecraft structure and radiation shields is a large part of the task.

The trapped proton and electron spectra are obtained by determining the position of the spacecraft in R-λ coordinates at predetermined time intervals, converting this position to B-L coordinates, and finding the flux spectra for each particle type at that position. The spectra are weighted by the fraction of time spent in each interval and then summed. The result is the total incident flux due to trapped protons and electrons as a function of energy over the life of the satellite. To this is added the appropriate solar proton spectrum based on the mission risk assessment. Understandably, this calculation is performed by computer.

The most efficient, but somewhat simplified, method for calculating the dose resulting from an incident spectrum uses SHIELDOSE,[10] a program developed at the National Institute of Standards and Technology. In preliminary calculations, various spacecraft components can be modeled using simple shield geometries, such as slabs or spheres of an average thickness. SHIELDOSE contains a database generated by Monte Carlo simulations of particle transport (including elastic and inelastic collisions, spallation, and electron energy loss from bremsstrahlung [secondary photons produced during the stopping of electrons]) for simple geometries in aluminum for many incident particle energies. Interpolation of this database

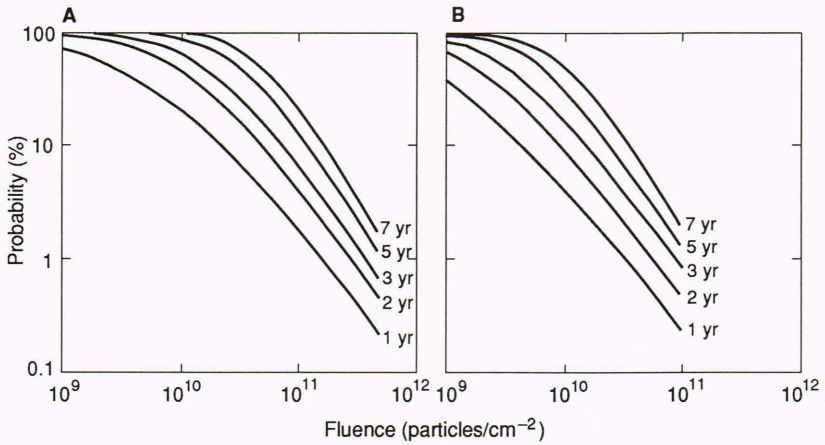

Figure 9. Probability of exceeding given fluence levels for mission lengths of one to seven years. **A.** Results for protons of energies >10 MeV. **B.** Results for protons of energies >30 MeV. (Reprinted, with permission, from Ref. 9: ©1990 by American Institute of Aeronautics and Astronautics.)

provides an accurate and rapid assessment of dose variation with shield thickness.

The SHIELDOSE code, however, is limited to solid or continuous geometric models for shields of a small number of materials. The use of other materials and the discontinuous configurations of spacecraft hardware require additional Monte Carlo simulation. This can be performed by the NOVICE code, which simulates individual particle histories by adjoint Monte Carlo analysis (particles are tracked backwards, speeding up the tracking process by ignoring particles with insufficient range to reach a given point). For simple shields, the histories are generated for a uniform infinite material and then overlaid on one-dimensional shield geometries by translation and rotation to obtain attenuation information for different shield thicknesses. In addition, SHIELDOSE uses the continually-slowing-down approximation for electron ionization. Therefore, large angle scattering of electrons is not considered. NOVICE adjoint Monte Carlo simulations avoid this approximation, and so treat the scattering of electrons more accurately.

A better dose estimate is obtained by accounting for the actual material distribution around a component. This distribution includes neighboring components, boards, boxes, enclosures, and subsystems. The most general description of the material distribution, applicable to various analyses, is a three-dimensional model. Each part of the spacecraft that can provide particle attenuation is described by material composition, shape (slabs, cylinders, cones, spheres, etc.), and dimensions.

In the dose analysis at a specific point, many solid angle elements are defined around the point, usually by a uniform mesh in azimuthal angle and polar angle cosine (e.g., a 60 $\times$ 30 mesh defines 1800 solid angle sectors). For each sector, a ray trace is performed from the dose point through the center of the sector to the outside of the spacecraft. The total mass thickness along the ray is then used to interpolate the dose–depth curve, and this interpolated dose, when multiplied by the fractional solid angle of the sector, estimates the dose of that sector. Repeating this process for all sectors, with a summation of the individual sector doses, gives an estimate of the total dose received at the point.

This ray trace/sectoring method can be applied to very detailed spacecraft models. For instance, the NOVICE code can perform calculations on a 200-component spacecraft model with over 1000 sectors per dose point in only a few minutes on a PC/workstation/MicroVax.

Unfortunately, even though the ray trace/sectoring method uses many details of the spacecraft construction, it remains an approximate methodology. Specifically, the path of the incoming radiation is approximated only by the materials encountered on straight-line paths through the solid angle sectors. This type of modeling is quite accurate for heavy ions (protons and galactic cosmic rays) since these particles travel in straight-line paths. For electrons and bremsstrahlung, however, the angular deflections of the particles are substantial. Therefore, the actual paths of the lighter particles can be quite tortuous. Often, these effects are not adequately modeled by the ray trace/sectoring methodology.

Two procedures are used to assess the actual dose levels when a radiation environment is dominated by trapped electrons. First, NOVICE sectoring models contain upper- and lower-bound dose estimates based on dose–depth curves for several idealized one-dimensional shield geometries. Second, NOVICE can perform a complete adjoint Monte Carlo simulation of the radiation levels at a specific point. This simulation uses the same geometric model analyzed by the ray trace/sectoring method and the same environmental model used in generating the one-dimensional dose–depth curves. Adjoint Monte Carlo analysis requires much more computer time than the sectoring analysis, typically several hours, and is only used for critical dose points.

Solar cell degradation is rarely studied in terms of ionizing dose in rads, so the preceding analysis does not generally apply. These devices are exposed to the bulk of the charged particle environment with little shielding. The low-energy particles that are normally attenuated by the shielding around a device degrade solar cells mainly through displacement damage of silicon atoms in the lattice. These defects create available states in the band gap of the solar cell diode, thereby increasing the dark current and reducing the power produced by the cell.

Displacement damage is best studied in terms of particle fluence. The damage caused by a given fluence of particles depends on their energy; lower-energy particles do comparably more damage than those with higher energy. Many experiments have been performed to identify damage equivalence factors, which are used to convert a fluence of particles at some energy to a fluence of particles at a standard energy doing equivalent damage.

By using these factors, the incident orbital spectrum is converted to a 1-MeV-equivalent electron fluence, and the damage done to a solar cell is then calculated. Various thicknesses of glass cover slides are available to block some of the very-low-energy particles, such as protons with energy below 1 MeV, which can stop in the solar cell and do the most damage. But a cover slide reduces the light available to the solar cell, which decreases the output of the array. Therefore, the solar array designer must choose a cover slide thickness that attenuates the lowest-energy particles and then design the array to accommodate the decrease in output resulting from displacement damage over the lifetime of the spacecraft.

SINGLE-EVENT PHENOMENA

High-energy particles (e.g., heavy ions found in galactic cosmic rays) traveling through an integrated circuit lose energy by creating electron–hole pairs. The electrons, being more mobile than the holes, are collected, forming a current pulse in the device. This current pulse can cause two problems: single-event upset and latchup. Latchup occurs when a device is put into a destructive high-current state by an interacting particle depositing charge within the bulk of the device below the active layers. A single-event upset is the reversal of the logic state of a memory cell caused by the deposition of charge in the active regions of a device, with consequences that vary from simple data errors to malfunctioning of a computer system. We have system-level solutions to many of the

problems caused by single-event phenomena, but proper engineering requires an accurate estimate of the upset and latchup rates for each component of a system that may be susceptible to single-event phenomena. As with total dose hardness assurance, a model of the environment and a way to calculate upset and latchup rates based on the model and ground-based component testing are needed.

Galactic cosmic rays are the primary source of energetic heavy ions found in Earth orbit. Figure 10 shows the unattenuated differential cosmic ray spectrum for a solar minimum epoch in the interplanetary medium as a function of energy per nucleon for several elements. Single-event phenomena, however, result from energy loss by a particle traveling through a material. Therefore, a more useful variable for characterizing the particle environment is linear energy transfer (LET), the rate at which energy is transferred to the target material along the path length, given by

$$S_e = \frac{dE}{dx} , \tag{3}$$

where S_e is the linear energy transfer, E is particle energy, and x is the distance along the path of the particle. Figure 11 gives the average galactic cosmic ray spectrum as a function of LET in the interplanetary environment for solar minimum conditions, which are based on measurements from several spacecraft.

The spectrum seen at a device, however, is attenuated by the effects of the Earth's magnetic field, shadowing by the Earth, and any shielding that may surround the device. Adams[11] developed a suite of computer programs called CREME, which transforms the model interplanetary energy spectra into the incident LET at a device for a particular orbit and shielding thickness. A plot of the attenuation owing to varying shield thickness generated using CREME is shown in Figure 12. Also, Figure 13 gives the effect of inclination on the orbit-averaged incident LET spectrum for a 400-km circular orbit behind a 0.17-g/cm^2 aluminum shield. In addition to the dependence on orbital inclination, the LET spectrum also varies as a function of altitude for low LET particles. These particles are rarely energetic enough to cause single-event phenomena, however, so that the altitudinal variations are not significant for low Earth orbit.[12]

In addition to an environmental model, single-event upset and latchup rate estimates require data on the susceptibility of devices to single-event phenomena. This susceptibility is usually measured in the form of the upset or latchup cross section σ, which is usually experimentally determined by exposing the device to a monoenergetic beam of heavy ions and counting the number of errors that occur. The cross section is then given by

$$\sigma = \frac{n}{\Psi} , \tag{4}$$

where Ψ is the total fluence seen by the device and n is the number of errors counted. The cross section is a

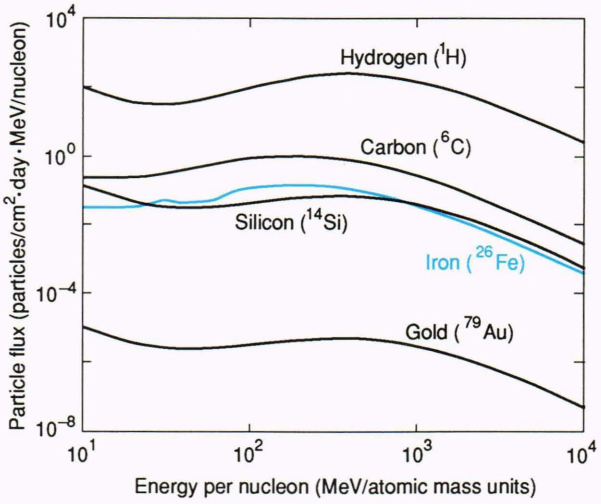

Figure 10. Unattenuated galactic cosmic ray flux as a function of energy for several ion species.

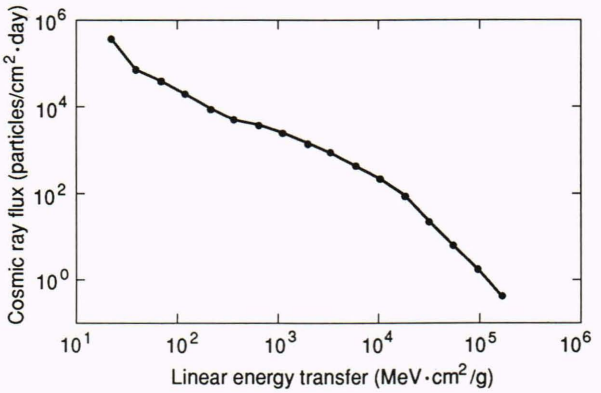

Figure 11. Average interplanetary galactic cosmic ray spectrum for solar minimum conditions behind 0.17 g/cm^2 of aluminum shielding.

function of LET and incident angle and has units of area. Figure 14 is a plot of a typical single-event upset cross section as a function of LET. For incident angles less than 70°, the cross section scales as $1/\cos\theta$, so several values of the cross section at different effective LET's can be measured by using a beam of nominal LET normal to the device and varying the angle of incidence.

Physically, the asymptotic value of the upset cross section is the area of the sensitive region within each flip-flop or memory cell that an incident particle must traverse to cause an upset. In addition, the threshold LET (L_T), that value at which upset begins to occur, is a measure of the critical charge necessary to cause a bit flip. An analytical approach to calculating the upset rate is given by assuming that the environment consists of particles with varying LET, some of which traverse the sensitive region of the device at random incident angles. The upset rate N is found by integrating the product of the flux spectrum with a differential path-length distribution through the sensitive volume, given by

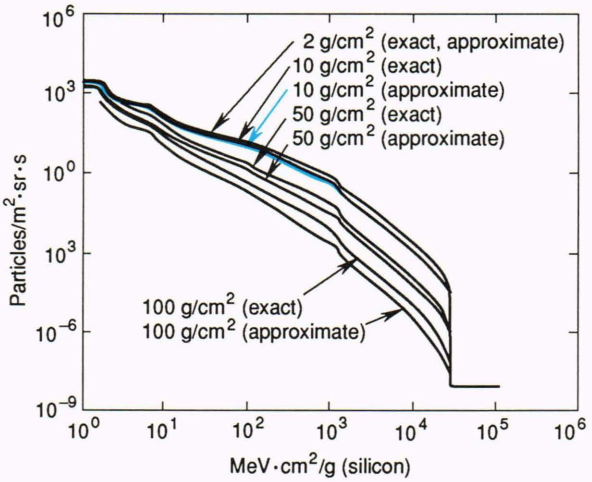

Figure 12. Integral LET spectra for galactic cosmic rays, including only those elements through iron. The results are given for an exact calculation of ion transport and for an approximate calculation that neglects the contribution of fragmented cosmic rays. (Reprinted, with permission, from Ref. 12, p. 4476: © 1983 by Institute of Electrical and Electronics Engineers.)

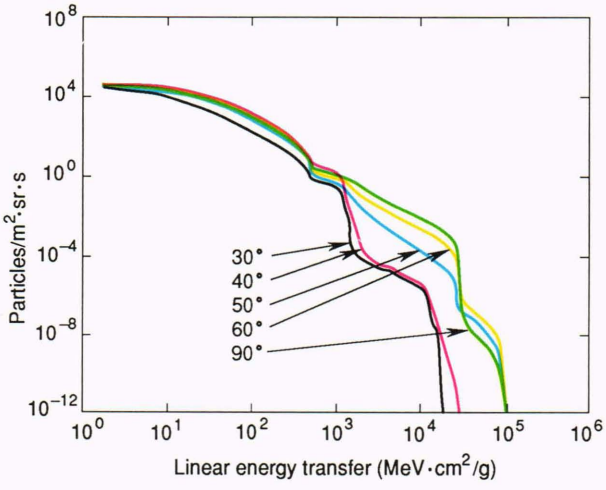

Figure 13. Integral LET spectra inside 0.17 g/cm² of aluminum shielding in a 400-km circular orbit for various orbital inclinations. (Reprinted, with permission, from Ref. 12, p. 4477: © 1983 by Institute of Electrical and Electronics Engineers.)

$$N = 22.5\pi\sigma_A Q_C \int_{L_T}^{L_{max}} \frac{1}{L^2} D[p(L)]F(L)\, dL\ , \qquad (5)$$

where

σ_A is the asymptotic cross section (the area of the sensitive region),

Q_C is the critical charge given by the threshold LET,

$D[p(L)]$ is the differential distribution of path lengths over which a particle of LET, L, will produce a charge greater than the critical charge, and

$F(L)$ is the environment.[13]

For space applications, $F(L)$ is the integral omnidirectional flux spectrum impinging on the spacecraft. This integral is usually performed numerically.

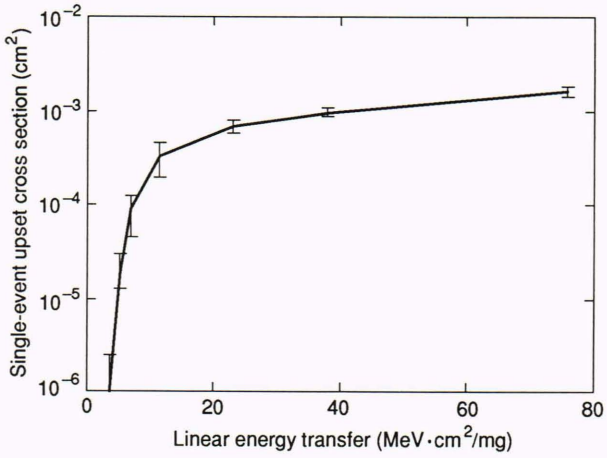

Figure 14. Typical single-event upset cross section as a function of LET.

This analytical method of error rate estimation depends on several assumptions:

1. Each memory cell or flip-flop within a device that can upset has a single sensitive region.
2. The sensitive region of each memory cell is a rectangular parallelepiped of known dimension. All sensitive regions are identical and have the same critical charge.
3. The single-event upset cross section of each sensitive region is a step function.

These assumptions model memories with regular structure very well but not complex devices such as microprocessors or signal processors. For instance, since the architecture of these latter devices is irregular, more than one size of sensitive region may exist, each with a different critical charge. Therefore, the upset cross section is rarely a step function. Since the environment contains many more particles in the LET range near the knee of the cross section, analytic calculations estimating this gradual knee by a step function in Equation 5 can overestimate the upset rate by as much as an order of magnitude. Even if we ignore these problems, correct application of the analytical method requires detailed information about the design and processing of a device (e.g., the thickness of active layers) that may not be available to its user. Finally, since latchup is a distinctly different mechanism, the analytical method is not appropriate for the calculation of latchup rates.

To avoid these problems, a probabilistic approach called MERGE was developed to calculate error rates directly from environmental and experimental cross-sectional data. An outline of the approach is as follows:

1. Normalize the experimentally determined cross section, a function of LET, by dividing by the total area of the integrated circuit.
2. Interpret the normalized cross section as a probability of upset for a given LET.
3. Within the framework of a computer simulation, allow a number of "particles" given by the expected environment to impinge on the "device" at random "angles."

4. Use the cosine approximation to correct the LET of each particle by the chosen angle.

5. Generate a random number to decide if each particle causes an upset, then count the total number of upsets.

6. Repeat the procedure a sufficient number of times to get a mean error rate and standard deviation.

This approach is easily applied and avoids the problems associated with analytic error rate calculations. In addition, it is not restricted to single-event upset calculations or memories, but could be applied equally well to other devices. An extension of MERGE could be used to examine the problem of calculating rates of system-level single-event phenomena on the basis of the device-level rates and information about the propagation of errors.

The MERGE approach offers several advantages for calculating single-event phenomena rates. First, MERGE requires only experimentally obtained data about the device in question. No information about the architecture or processing of the integrated circuit is needed. In addition, the accuracy of MERGE does not depend on assumptions about the shape and size of the sensitive regions. Finally, the entire cross-sectional curve is used, so overestimation of the error rate resulting from the step function assumption does not occur.

The Monte Carlo approach used in MERGE has several disadvantages. The results depend heavily on the quality of the cross-sectional data and environmental model. The MERGE approach requires more data than the CREME approach. In addition, the accuracy of the calculation depends on the quality of the random-number generator employed. Finally, unlike the CREME approach, MERGE gives no new information on how to improve device single-event phenomena sensitivity. None of these problems significantly detracts from the usefulness of MERGE and the improved error rate estimates, however.

APPLICATIONS

The total dose estimation methodology described here has been applied to a recent Applied Physics Laboratory instrument, Energetic Particle and Ion Composition (EPIC), to be flown on the Geotail spacecraft. Figure 15 gives the layout of the Geotail upper deck on which EPIC is mounted. The initial radiation analysis using SHIELDOSE gave an upper bound of the total dose hardness requirement of 30 krad (silicon) for moderate shield thicknesses. Weight reduction became critical, however, so a more detailed calculation of the dose within each electronics box was needed. A computer model of the Geotail spacecraft layout was built, and the NOVICE ray trace/sectoring algorithm was applied. A plot of the dose within one of the EPIC boxes is shown in Figure 16. Similar analyses were run for several box thicknesses, and the results were used to select the optimum wall thickness for shielding while minimizing the weight of the electronics boxes. In addition, the dose maps indicated the best positions within each box for more sensitive components, further reducing the amount, and thereby the weight, of component shielding.

The Harris 80C86RH microprocessor was considered for use in a spacecraft command system. For reliability, the single-event upset rate had to be low, so an estimate of the upset rate was needed to evaluate the use of the 80C86RH. Sample devices were exposed to heavy ions at Brookhaven National Laboratory in a configuration resembling a command system computer running flight software, and the upset cross section was measured as a function of LET, as shown in Figure 14. CREME was used to generate an estimate of the orbital flux spectrum for a 900-km polar orbit during solar minimum. The environmental and cross-sectional data were used by MERGE to calculate the expected upset rate. For a 90% worst-case environment (actual conditions worse only 10% of the time), the error rate was 0.2 error/day, or one upset every five days. This rate was considered too

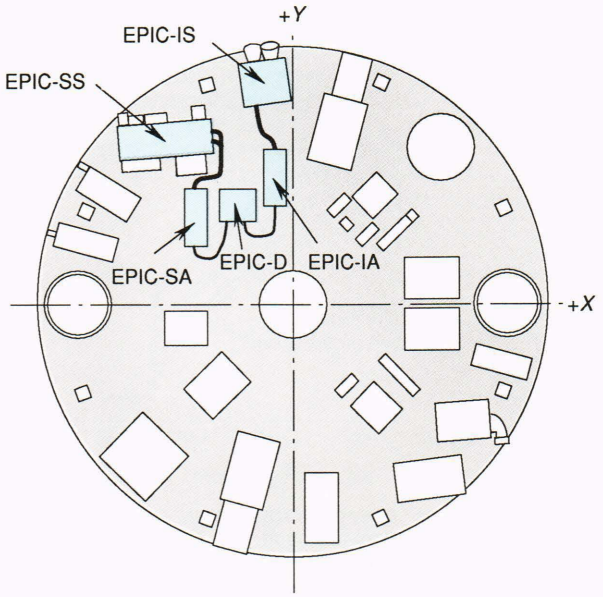

Figure 15. The upper deck of the Geotail spacecraft, indicating the mounting position of the EPIC boxes. (SA = sensor electronics; D = data processing unit; IS = instrument sensor; SS = controller; IA = interface electronics.)

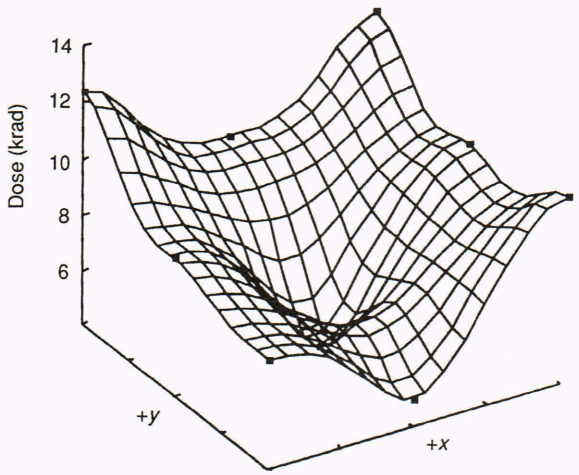

Figure 16. Dose profile in the upper layer (just below the box lid) of the EPIC-IA (interface electronics) box with 0.6-mm aluminum walls.

high for reliable command system operation, so another device was used. Nevertheless, use of the 80C86RH in noncritical instrument applications is still planned.

The Analog Devices ADSP2100A is a digital signal processor currently used for image processing in a satellite tracking system. When exposed to a heavy ion beam, test samples of this device latched up, a condition wherein the device power is shorted to ground through the body of the integrated circuit. The large currents that pass through the device during latchup are usually damaging unless the device is protected. The orbital latchup rate estimate given by MERGE indicated that the latchup rate would not exceed ten events per year. This rate was acceptable for the image processing system if adequate latchup protection could be implemented at the system level. Therefore, the image processing computer, which uses the ADSP2100A, was designed to detect a latched condition and remove power from the device before any damage could occur.

Some devices sensitive to single-event phenomena can be upset by protons found in the Van Allen radiation belts. Recently, the 93L422 static random access memories used on the Hubble Space Telescope have been observed to upset in the SAA at an average rate of once per day. To validate the MERGE simulation, an estimate of the expected upset rate based on cross-sectional data taken before the Hubble launch was calculated. Using an average proton spectrum, the expected proton upset rate for the 93L422 given by MERGE is 0.6 error/day. However, the proton environment is an average for periods of time greater than six months; the proton flux can vary by as much as a factor of 3 on shorter time scales. Given such a large deviation from the average, we feel that the 40% difference between the estimated and observed error rate is quite good.

CONCLUSIONS

We have discussed the methods and tools that are used to make predictions of total dose and single-event phenomena rates for satellite systems in Earth orbit. These tools give accurate information for use in the design of systems that can survive the radiation in space without suffering undue penalties in performance. Often NOVICE and MERGE have proven valuable and will continue to be used in future programs.

Two areas still need to be addressed. First, the problem of system-level propagation of component-level errors has been neglected. It is not clear that all errors in devices propagate through a system. Also, an error in one device may cause multiple system errors. Therefore, the system-level error rate may not be just the algebraic sum of the component-level error rates. These effects should be studied further, and MERGE should be extended to simulate system effects as well. Finally, even though recent flight data have validated the MERGE simulation, more flight data concerning the actual dose and single-event upset rates in space must be gathered to refine current models and monitor the range of dynamic changes over the life of a spacecraft mission. To this end, total dose and single-event upset monitors are being designed for several upcoming APL satellite systems. In addition, several NASA satellites such as the Chemical Release Radiation Effects Satellite (launched in July 1990) will also return total dose and single-event upset data, which will be used to improve the tools needed for system hardness assurance.

REFERENCES

[1] Van Allen, J. A., Ludwig, G. H., Ray, E. C., and McIlwain, C. E., "Observations of High Intensity Radiation by Satellites 1958 Alpha and Gamma," *Jet Propul.* **28** (1958).

[2] Knecht, D. J., and Shuman, B. M., "The Geomagnetic Field," in *The Handbook of Geophysics and the Space Environment,* Jursa, A. S., ed., AFGL-TR-85-0315, Air Force Geophysics Laboratory, Hanscom AFB, Mass., pp. 4-1–4-37 (1985).

[3] Alfvén, H., and Falthammar, C. G., *Cosmical Electrodynamics*, Clarendon Press, Oxford, U.K. (1963).

[4] Schulz, M., and Lanzerotti, L. J., *Particle Diffusion in the Radiation Belts*, Springer-Verlag, New York (1974).

[5] Spjeldvik, W. N., and Rothwell, C. G., "The Radiation Belts," in *The Handbook of Geophysics and the Space Environment,* Jursa, A. S., ed., AFGL-TR-85-0315, Air Force Geophysics Laboratory, Hanscom AFB, Mass., pp. 5-1–5-55 (1985).

[6] Sawyer, D. M., and Vette, J. I., *AP-8 Trapped Proton Environment for Solar Maximum and Solar Minimum*, NSSDC/WDC-A-R&S, National Science Data Center, Greenbelt, Md. (1976).

[7] King, J. H., "Solar Proton Fluences for 1977–1983 Space Missions," *J. Spacecr. Rockets* **11**, 401 (1974).

[8] Feynman, J., Armstrong, T. P., Dao-Gibner, L., and Silverman, S., "A New Proton Fluence Model for E > 10 MeV," in *Proc. Interplanetary Particle Environment Conf.,* NASA, p. 58 (1988).

[9] Feynman, J., and Gabriel, S., "A New Model for Calculation and Prediction of Solar Proton Fluences," in *Proc. 28th Aerospace Sciences Meeting,* American Institute of Aeronautics and Astronautics, Reno, Nev. (8–11 Jan 1990).

[10] Seltzer, S., *SHIELDOSE: A Computer Code for Space Shielding Radiation Dose Calculations*, NBS TN-1116, National Bureau of Standards (1980).

[11] Adams, J. R., *Cosmic Ray Effects on Microelectronics, Part IV,* NRL-5901, Naval Research Laboratory, Washington, D.C. (31 Dec 1986).

[12] Adams, J. R., "The Variability of Single Event Upset Rates in the Natural Environment," *IEEE Trans. Nucl. Sci.* **30**, 4475–4480 (1983).

[13] Petersen, E. L., Shapiro, P., Adams, J. H., and Burke, E. A., "Calculation of Cosmic Ray Induced Soft Upsets and Scaling in VLSI Devices," *IEEE Trans. Nucl. Sci.* **29**, 2055–2063 (1982).

THE AUTHORS

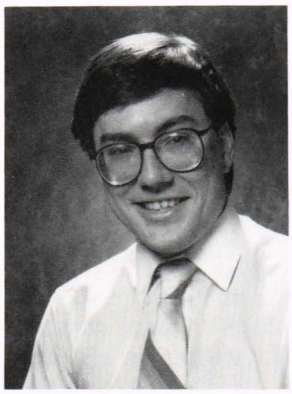

JAMES D. KINNISON received a B.Sc. in physics from Northeast Louisiana University in 1984 and an M.Sc. in elementary particle physics from Michigan State University in 1987. While at Michigan State University, Mr. Kinnison designed several particle detector systems for high-energy particle physics experiments at Fermi National Accelerator Laboratory. Since 1987, Mr. Kinnison has been a member of the Associate Professional Staff at APL working in the Satellite Reliability Group. In that position, he primarily studies the problem of accurately predicting the response of electronic systems to the particle environment found in space.

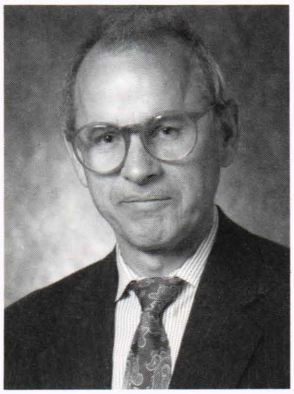

THOMAS M. JORDAN received a B.Sc. from the University of Missouri at Rolla in 1960. In 1960–61, he attended the University of Illinois as a National Science Foundation Fellow in Physics. From that time until 1972, Mr. Jordan held several positions studying satellite hardening and radiation effects in manned space missions, nuclear weapons effects, and portable reactor technology. Since 1972, he has served as consultant for over thirty government and aerospace organizations. He is a member of the American Physical Society, Institute of Electrical and Electronics Engineers, and American Nuclear Society.

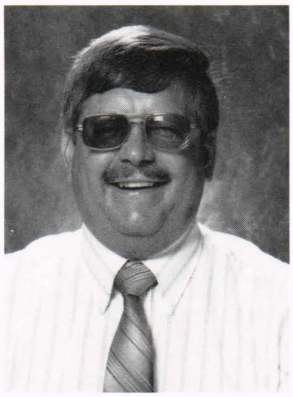

RICHARD H. MAURER received a Ph.D. in theoretical particle physics from the University of Pittsburgh in 1970. He spent three years as a postdoctoral fellow in cosmic ray physics at the Bartol Research Foundation in Swarthmore, Pennsylvania. Dr. Maurer joined APL in 1981 and is a member of the Principal Professional Staff and the Space Department Reliability Group. His publications include articles on antiproton production, extensive air showers, total dose effects on digital logic devices and quartz crystal resonators, permanent radiation damage to silicon and gallium arsenide solar cells, single-event effects in very large scale integrated devices, safety aspects of lithium batteries, spacecraft electronics packaging, and reliability studies of gallium arsenide transistors.